Results from KASCADE-Grande

, ,
, ,
; ; ;

Results from KASCADE-Grande

M. Bertaina[a,q], W.D. Apel[b], J.C. Arteaga-Velázquez[c], K. Bekk[b], J. Blümer[b,d], H. Bozdog[b], I.M. Brancus[e], P. Buchholz[f], E. Cantoni[a,g], A. Chiavassa[a], F. Cossavella[d,m], K. Daumiller[b], V. de Souza[h], F. Di Pierro[a], P. Doll[b], R. Engel[b], J. Engler[b], M. Finger[d], D. Fuhrmann[i], P.L. Ghia[g], H.J. Gils[b], R. Glasstetter[i], C. Grupen[f], A. Haungs[b], D. Heck[b], J.R. Hörandel[j], D. Huber[d], T. Huege[b], P.G. Isar[b,n], K.-H. Kampert[i], D. Kang[d], H.O. Klages[b], K. Link[d], P. Łuczak[k], M. Ludwig[d], H.J. Mathes[b], H.J. Mayer[b], M. Melissas[d], J. Milke[b], B. Mitrica[e], C. Morello[g], G. Navarra[a,o], J. Oehlschläger[b], S. Ostapchenko[b,p], S. Over[f], N. Palmieri[d], M. Petcu[e], T. Pierog[b], H. Rebel[b], M. Roth[b], H. Schieler[b], F.G. Schröder[b], O. Sima[l], G. Toma[e], G.C. Trinchero[g], H. Ulrich[b], A. Weindl[b], J. Wochele[b], M. Wommer[b], J. Zabierowski[k]

[a] *Dipartimento di Fisica Generale dell' Università Torino, Italy*
[b] *Institut für Kernphysik, KIT - Karlsruher Institut für Technologie, Ger many*
[c] *Universidad Michoacana, Instituto de Física y Matemáticas, Morelia, Mexico*
[d] *Institut für Experimentelle Kernphysik, KIT - Karlsruher Institut für Technologie, Germany*
[e] *National Institute of Physics and Nuclear Engineering, Bucharest, Romania*
[f] *Fachbereich Physik, Universität Siegen, Germany*
[g] *Istituto di Fisica dello Spazio Interplanetario, INAF Torino, Italy*
[h] *Universidade São Paulo, Instituto de Física de São Carlos, Brasil*
[i] *Fachbereich Physik, Universität Wuppertal, Germany*
[j] *Dept. of Astrophysics, Radboud University Nijmegen, The Netherlands*
[k] *Soltan Institute for Nuclear Studies, Lodz, Poland*
[l] *Department of Physics, University of Bucharest, Bucharest, Romania*
[m] *now at: Max-Planck-Institut Physik, München, Germany*
[n] *now at: Institute Space Sciences, Bucharest, Romania*
[o] *deceased*
[p] *now at: Univ Trondheim, Norway*
[q] *corresponding author: bertaina@to.infn.it*

Abstract

The KASCADE-Grande experiment, located at Karlsruhe Institute of Technology (Germany) is a multi-component extensive air-shower experiment devoted to the study of cosmic rays and their interactions at primary energies 10^{14} - 10^{18} eV. Main goals of the experiment are the measurement of the all-particle energy spectrum and mass composition in the 10^{16} - 10^{18} eV range by sampling charged (N_{ch}) and muon (N_{μ}) components of the air shower. The method to derive the energy spectrum and its uncertainties, as well as the implications of the obtained result, is discussed. An overview of the analyses performed by KASCADE-Grande to derive the mass composition of the measured high-energy comic rays is presented as well.

Keywords: cosmic rays, energy spectrum, composition, 10^{16} - 10^{18} eV, KASCADE-Grande

1. Introduction

The study of the energy spectrum and of the chemical composition of cosmic rays are fundamental tools to understand origin, acceleration and propagation of cosmic rays. The energy range between 10^{16} eV and 10^{18} eV is quite important from astrophysical point of view because it is expected that in this energy range the transition between galactic and extra-galactic origin of cosmic rays will occur. The results obtained at lower energies by KASCADE (1) and EAS-TOP (2) as well as by other experiments suggest that the knee in the primary energy spectrum around $3 - 4 \times 10^{15}$ eV is due to the break in the spectra of elements with light mass ($Z < 6$). Several models forsee a rigidity dependence of such breaks. Therefore, a knee of the heaviest components would be expected in the range of 10^{16} eV to 10^{18} eV. Various theories with different assumptions try to explain the rather smooth behavior of the cosmic ray energy spectrum in this energy range (i.e. (3; 4)). In order to discriminate between the different models, a very precise measurement of the possible structures of the energy spectrum and of the evolution of the composition is needed.

2. The apparatus

The KASCADE-Grande experiment (5) (see figure 1) is a multi-detector setup consisting of the KASCADE experiment (6), the trigger array Piccolo and the scintillator detector array Grande. Additionally, KASCADE-Grande includes an array of digital read-out antennas, LOPES (7; 8), to study the radio emission in air showers at $E > 10^{17}$ eV. Most important for the analysis presented here are the two scintillator arrays: KASCADE and Grande. The KASCADE array comprises 252 scintillator detector stations structured in 16 clusters. The detector stations house two separate detectors for the electromagnetic (unshielded liquid scintillators) and muonic components

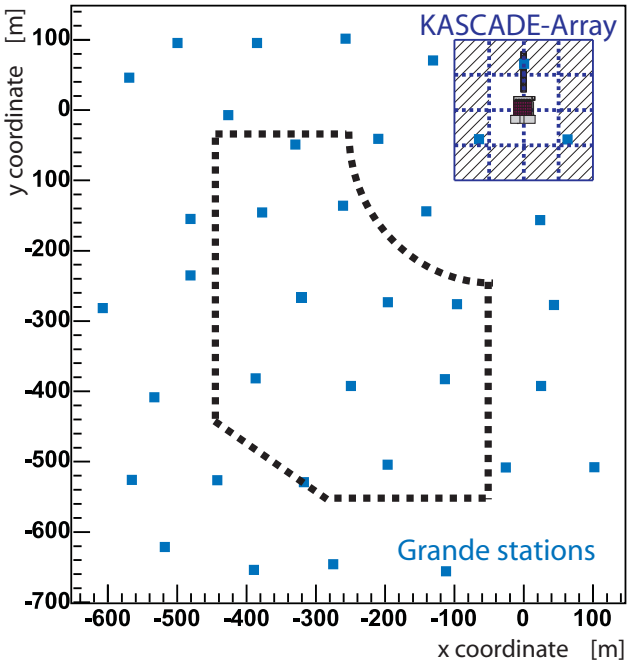

Figure 1: Layout of the KASCADE-Grande experiment: The original KASCADE and the distribution of the 37 stations of the Grande array are shown. The outer 12 clusters of the KASCADE array employ also shielded μ-detectors. The dashed line shows the area used in the present analysis.

(shielded plastic scintillators) where muon detectors are housed in 12 clusters (or 192 stations), only. This enables to reconstruct the lateral distributions of muons and electrons separately on an event-by-event basis. The Grande array is formed by 37 stations of plastic scintillator detectors, 10 m^2 each (divided into 16 individual scintillators) spread on a 0.5 km^2 surface, with an average grid size of 137 m. Grande is arranged in 18 hexagonal clusters formed by 6 external detectors and a central one. Grande and KASCADE arrays are both triggered when all the 7/7 stations in a hexagon have fired (rate $\sim$ 0.5 Hz). Full efficiency for proton and iron primaries is reached at $\log N_{ch} > 5.8$. For a subsample of events collected by the Grande array it is possible to compare on an event-by-event basis the two independent reconstructions of KASCADE and Grande. By means of such a comparison the Grande reconstruction accuracies are found to be for the shower size: systematic uncertainty $\leq$ 5%, statistical inaccuracy $\leq$ 15%; for arrival direction: $\sigma \approx 0.8°$; for the core position: $\sigma \approx$ 6 m (5). All of them are in good accordance with the resolutions obtained from simulations.

3. The analysis

The technique employed to derive the all-particle energy spectrum and its mass composition is based on the correlation between the size of the charged particles (N_{ch}) and muons (N_μ) on an event-by-event basis. The method itself has been described in detail in (9). Here, we summarize the main points.

A sample of Monte Carlo data was simulated including the full air shower development in the atmosphere, the response of the detector and its electronics as well as their uncertainties. In this way, the parameters reconstructed from simulation are obtained in the same way as for real data. The EAS events were generated with an isotropic distribution with spectral index $\gamma = -3$ and were simulated with CORSIKA (10) and the hadronic Monte Carlo generators FLUKA (11) and QGSJet II-03 (12). Sets of simulated events were produced in the energy range from 10^{15} eV to 10^{18} eV with high statistics and for five elements: H, He, C, Si and Fe, representative for different mass groups ($\approx$ 353.000 events per primary). Few events up to $3 \cdot 10^{18}$ eV were also generated in order to cross-check the reconstruction behavior at the highest energies.

Grande stations (5) are used to provide core position and angle-of-incidence, as well as the total number of charged particles in the shower, by means of a maximum likelihood procedure comparing the measured number of particles with the one expected from a modified NKG lateral distribution function (13) of charged particles in the EAS.

The total number of muons is calculated using the core position determined by the Grande array and the muon densities measured by the KASCADE muon array detectors. The total number of muons N_μ in the shower disk (above the energy threshold of 230 MeV) is derived from a maximum likelihood estimation assuming a lateral distribution function based on the one proposed by Lagutin and Raikin (14). The reconstruction procedures and obtained accuracies of KASCADE-Grande observables are described in detail in reference (5).

For the reconstructed events, we restricted ourselves to events with zenith angles lower than 40°. Additionally, only air showers with cores located in a central area on KASCADE-Grande were selected. With this cut on the fiducial area, border effects are discarded and possible under- and overestimations of the muon number for events close to and far away from the center of the KASCADE array are reduced. All of these cuts were applied also to the Monte Carlo simulations to study the effects and to optimize the cuts. Full efficiency for triggering and reconstruction of air-showers is reached at primary energy of $\approx 10^{16}$eV, slightly depending on the cuts needed for the reconstruction of the different observables (5).

The analysis presented here is finally based on 1173 days of data and the cuts on the sensitive central area and zenith angle correspond to a total acceptance of $A = 1.976 \cdot 10^9$ cm$^2\cdot$ sr, and an exposure of $N = 2.003 \cdot 10^{17}$ cm$^2\cdot$ s$\cdot$sr, respectively.

With Monte Carlo simulations a formula is obtained to calculate the primary energy per individual shower on the basis of N_{ch} and N_μ. The formula takes into account the mass sensitivity in order to minimize the composition dependence in the energy assignment, and at the same time, provides an event-by-event separation between electron-rich and electron-poor candidates. The formula is defined for 5 different zenith angle intervals ($\theta <$ 16.7, 16.7 $\leq \theta <$ 24.0, 24.0 $\leq \theta <$ 29.9, 29.9 $\leq \theta <$ 35.1, 35.1 $\leq \theta <$ 40.0) independently, to take into account the shower attenuation in atmosphere. Data are combined only at the very last stage to obtain a unique power law spectrum and mass composition.

The energy assignment is defined as $E = f(N_{ch}, k)$ (see equation 1), where N_{ch} is the size of the charged particle com-

Table 1: Parameters of the calibration functions.

Angles[deg]	a		b		c		d	
	H	Fe	H	Fe	H	Fe	H	Fe
0.0 – 16.7	0.910	0.876	1.333	1.817	0.100	0.161	0.786	-0.055
16.7 – 24.0	0.894	0.878	1.495	1.923	0.081	0.179	0.884	-0.254
24.0 – 29.9	0.937	0.889	1.301	1.935	0.104	0.156	0.677	-0.170
29.9 – 35.1	0.934	0.881	1.458	2.099	0.109	0.171	0.543	-0.351
35.1 – 40.0	0.919	0.875	1.748	2.287	0.105	0.156	0.412	-0.348

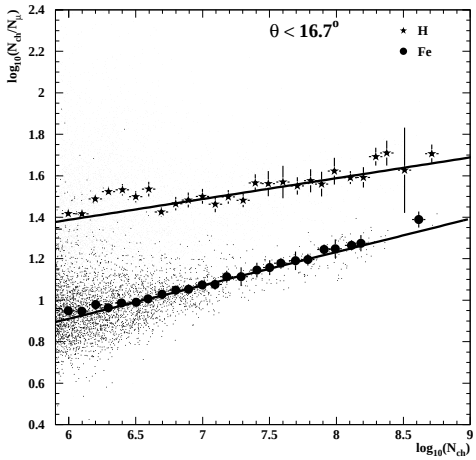

Figure 2: Scatter plot of the reconstructed N_{ch}/N_{μ} vs. N_{ch} for H and Fe primaries for the first angular bin. The full dots and error bars indicate the mean and its statistical error of the distribution of the individual events (small dots). The fits result in parameters c and d of expression 3.

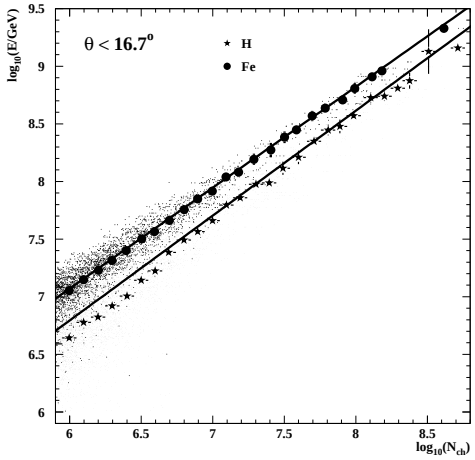

Figure 3: Scatter plot of E vs. N_{ch} for Fe and H primaries. The fits result in parameters a and b of expression 1.

ponent and the parameter k is defined through the ratio of the sizes of the N_{ch} and muon (N_{μ}) components: $k = g(N_{ch},N_{\mu})$ (see equation 2). The main aim of the k variable is to take into account the average differences in the N_{ch}/N_{μ} ratio among different primaries with same N_{ch} and the shower to shower fluctuations for events of the same primary mass:

$$log_{10}(E[GeV]) = [a_H + (a_{Fe} - a_H) \cdot k] \cdot log_{10}(N_{ch}) + b_H + (b_{Fe} - b_H) \cdot k \quad (1)$$

$$k = \frac{log_{10}(N_{ch}/N_{\mu}) - log_{10}(N_{ch}/N_{\mu})_H}{log_{10}(N_{ch}/N_{\mu})_{Fe} - log_{10}(N_{ch}/N_{\mu})_H} \quad (2)$$

$$log_{10}(N_{ch}/N_{\mu})_{H,Fe} = c_{H,Fe} \cdot log_{10}(N_{ch}) + d_{H,Fe}. \quad (3)$$

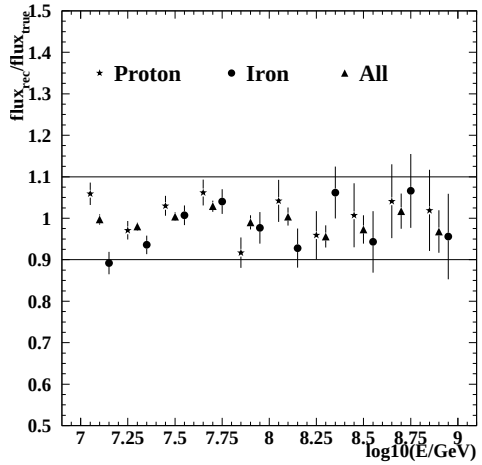

Figure 4: Ratio between the reconstructed and true simulated energy spectra for H, Fe and all mixed primaries summing up all angular bins.

Figs. 2, 3 show the scatter plots with the parametrizations defined for H and Fe in the first angular bin, while table 1 the summarizes the complete list of parameters *a* -*d*. Fig. 4 shows the capability of reproducing simulated energy spectra. Pure spectra of H, Fe and a mixture of 5 different primaries with 20% abundance each are shown as examples. The true flux is always reproduced within 10% uncertainty.

The k parameter is, by definition of eq. (2), a number centered around 0 for H showers and 1 for Fe ones if expressed as a function of N_{ch}, while slightly shifted when reported as a function of energy (see Fig. 8). After applying the procedure to the 5 angular bins independently, a combined spectrum is obtained by using all the events of the 5 bins calibrated with their own calibration function. A smoothing procedure is also applied to take into account the shower fluctuations. Systematic uncertainties due to the following reasons were considered: a) different intensity in the five angular bins, b) capability of reproducing an, a priori assumed, single primary spectrum with slope $\gamma = -3$, c) uncertainty on the index of the energy spectrum used to derive the energy relation $E(N_{ch})$ and the response matrix, d) uncertainty on the core location. The total uncertainty is around 15% and it is quite stable in the entire energy range. Regarding the energy resolution, it varies between 26% at the threshold

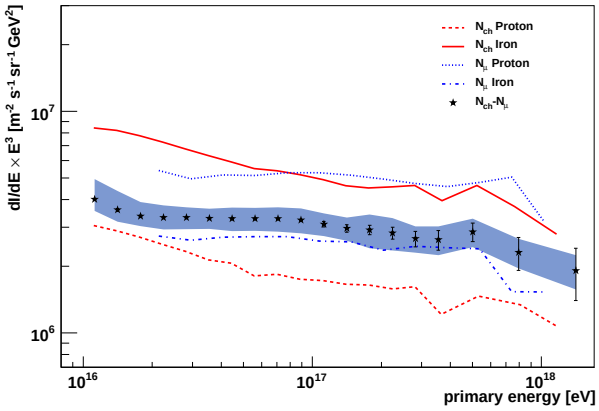

Figure 5: Reconstructed all-particle energy spectrum by the three different methods applied to KASCADE-Grande data. For the $N_{ch} - N_{\mu}$ method a band is shown indicating the range of the systematic uncertainty.

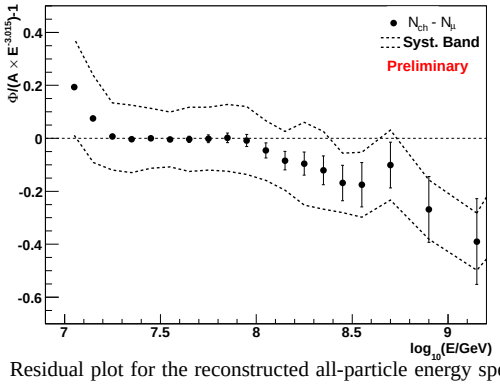

Figure 6: Residual plot for the reconstructed all-particle energy spectrum obtained from KASCADE-Grande through the N_{ch} - N_{μ} method. The systematic error band is also shown (dotted lines).

and 20% at the highest energies due to the decrease of the intrinsic shower fluctuations.

4. The energy spectrum

Using the N_{ch}-N_{μ} ratio we reduced the dependence of the reconstructd all-particle spectrum on the elemental composition. But, since both observables are reconstructed independently, we can apply an energy reconstruction on both observables individually. At first the shower size spectra are reconstructed, then an attenuation correction is applied to the observables. Finally, the shower size per individual event is calibrated by Monte Carlo simulations under the assumption of correlations in the form $E_0 \propto N_{ch}^{\alpha_{ch}}$ and $E_0 \propto N_{\mu}^{\alpha_{\mu}}$, respectively, and an assumed primary composition (15; 16).
In Figure 5 the spectra obtained by the three methods are compiled, where the flux is multiplied by a factor E^3. Owing to the different approaches, the results using single observables are obtained only for pure proton and iron assumptions, whereas the final spectrum is displayed with a band showing the systematic uncertainties. Taking into account the uncertainties, in particular due to the unknown composition, which in fact is the main source of the large band of single observable spectra, there is a fair agreement between the all-particle energy spectra obtained by the different approaches.

Despite the overall very smooth power law behavior of the resulting all-particle spectrum, there are some smaller structures observed, which does not allow to describe the spectrum with a single slope index. Figure 6 shows the resulting all-particle energy spectrum multiplied with a factor that the middle part of the spectrum is flat. Just above 10^{16} eV the spectrum shows a "concave" behavior, which is significant with respect to the systematic and statistical uncertainties. Another feature visible in the spectrum is a small break at around 10^{17} eV. A fit with a power law spectrum above 10^{17} eV gives a spectral index of $\gamma = -3.24 \pm 0.08$.
As the change of spectral index is small compared to the main knee, a significant conclusion is not possible without investigating the composition in detail in this energy range. These composition studies are presently underway at KASCADE-Grande adopting different approaches based on N_{ch} and N_{μ} observables, among them: a) the reconstruction of the local muon densities at a certain distance to the shower core as it gives a sensitivity to changes in the elemental composition (17); b) the distributions of the N_{ch}/N_{μ} ratio (18) as a function of N_{ch} ; c) the evolution of the variable $Y = log(N_{ch})/log(N_{\mu})$ as a function of energy (19); d) the evolution of the variable k as defined in equation 2; e) an unfolding procedure, similar to what was already performed with the KASCADE data (20).

5. The composition studies

The influence of predictions of the hadronic interaction models has a much larger influence on the composition than on the primary energy. The relative abundances of the individual elements or elemental groups is very dependent on the hadronic interaction model used to derive the energy spectrum of the single mass groups. However, the structures or characteristics of these spectra are found to be much less affected by the differences of the various hadronic interaction models than the relative abundance. The present goal is to verify the structure found in the all-particle energy spectrum around 100 PeV in the individual mass groups spectra and to assign it to a particular mass.

The muon densities (17): Muons are the messengers of the hadronic interactions of the particles in the shower and therefore are a powerful tool to determine the primary particle mass and to study the hadronic interaction models. For each shower, the density of muons is calculated as follows. The muon stations are grouped in rings of 20 m distance from the shower axis. The sum of the signals measured by all muon stations inside each ring is divided by the effective detection area of the stations. Therefore the muon density as a function of the distance from the shower axis is measured in a very direct way. No fitting of lateral distributions is needed in these calculations. The total number of electrons in the shower is reconstructed in a combined way using KASCADE and KASCADE-Grande stations. A lateral distribution function (LDF) of the

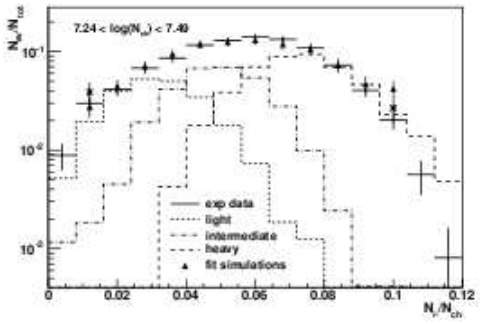

Figure 7: Shower size ration distributions for a certain bin in charged particle number. Shown is the measured distribution as well as the simulated ones for three primary mass groups and the resulting sum.

Lagutin type can be fitted to the density of muons measured by the KASCADE detector. After that, using the fitted function, the number of muons at any distance from the shower axis can be estimated. The KASCADE-Grande stations measure the number of charged particles. The number of electrons at each KASCADE-Grande stations is determined by subtracting from the measured number of charged particles the number of muons estimated with the LDF fitted to the KASCADE stations. Finally, the muon densities are plotted as a function of the electron number and compared with Monte Carlo expectations using specific hadronic interaction models for primaries of different mass.

Charged particle vs muon number ratio (18): The total number of charged particles N_{ch} and the total number of muons N_μ of each recorded event are considered and the distribution of N_μ/N_{ch} is studied in different intervals of N_{ch} (corresponding to different energy intervals) and zenith angle. The experimental distribution of the observable N_μ/N_{ch} is taken into account and fitted with a linear combination of elemental contributions from simulations, where we distinguish three groups: light, medium and heavy primaries. By this way the means and the widths of the distributions as two mass sensitive observables are taken into account (see as an example in figure 7). The width of the data distribution is in all ranges of N_{ch} so large that always three mass groups are needed to describe them. Using the Monte Carlo simulations the corresponding energy of each mass group and shower size bin is assigned to obtain the spectra of the individual mass groups.

The Y-cut method (19): Here, the shower ratio Y_{CIC} = log N_μ/log N_{ch} between the muon and the charged particle numbers, both corrected for atmospheric attenuation by the Constant Intensity Cut method (CIC), is used as parameter to separate the KASCADE-Grande data into different mass groups. MC simulations performed with CORSIKA on the framework of FLUKA/QGSJET-II are employed to obtain the expected Y_{CIC} distributions as a function of the energy for different cosmic ray primaries as a basis for the separation. Then the Y_{CIC}-parameter is used to divide the KASCADE-Grande data into electron-rich and electron-poor events, i.e. generated by light and heavy primaries.

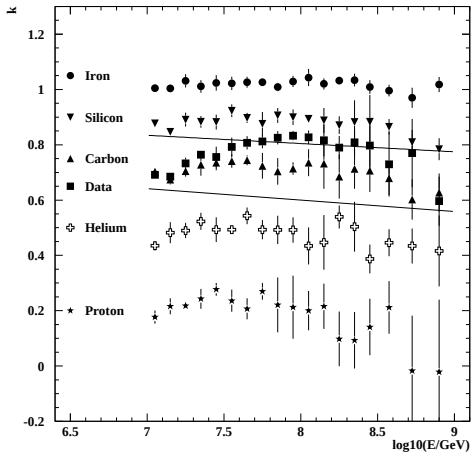

Figure 8: Evolution of the *k* parameter as a function of the reconstructed energy for experimental data compared with pure primary spectra for the entire angular range 0-40°.

The Gold-unfolding method (20): This method is based on the unfolding of the two-dimensional shower size spectrum in a similar way as it was developed for the KASCADE data analysis (1). Due to the fact that the accuracy in reconstructing the shower sizes for KASCADE-Grande are not as high as in case of KASCADE, the unfolding can be performed in three mass groups, only. Nevertheless, the resulting individual mass group spectra can be combined to provide a solution for the entire energy range from 1 PeV to 1 EeV.

The k-parameter method: Fig. 8 shows, after averaging all angular bins together, the evolution of the *k* parameter as a function of the reconstructed energy obtained by simulating with QGSJet II-03 model pure H, He, C, Si, Fe primary spectra, as well as for the experimental data. Similar behavior is obtained if each angular bin is analyzed separately. The error bars indicate the average dispersion of the *k* parameter among different bins, which include statistical errors, and systematic uncertainty of equations 3 in each angular bin. Fig. 8 shows also two straight lines which are used to classify events into different mass groups. The classification is done by defining specific lines for each angular bin, independently, to avoid possible systematic effects among the bins. However, we explain in the following the general concept, referring to Fig. 8. The top line represents the separation between 'heavy' and 'medium' groups and it is defined by fitting the $k_h(E) = (k_{Si}(E) + k_C(E))/2$ points which are obtained by averaging the values of *k* for Si and C components. In analogy, the bottom line represents the separation line between 'medium' and 'light' groups and it is defined by fitting the $k_l(E) = (k_C(E) + k_{He}(E))/2$ points which are obtained by averaging the values of *k* for C and He components. In the following, 'heavy' events will be defined as those having a *k* value higher than the top line and 'light' events those with *k* below the bottom line. The region in between, which is dominated mainly by CNO and highly contaminated by Si and He, will be defined as the 'medium' component. Such an assignment is, therefore, chosen on an event-by-event basis. Naturally, the ab-

solute abundances of the events in the three classes depend on the location of the straight lines. However, the evolution of the abundances as a function of energy will be retained by this approach, as the lines are defined through a fit to the *k* values.
The result that can be derived from fig. 8, is that in the framework of the QGSJet II-03 model, the region between 10^{16} and 10^{18} eV shows an average value of *k* compatible with 'medium' and 'heavy' candidates. The average value of *k* is increasing as a function of energy and reaches a plateau around 10^{17}. This plateau is located at the same place where a change in the spectral index is observed in the all-particle spectrum (see also the residual plot of the all-particle energy spectrum of KASCADE-Grande in fig. 6).

6. Conclusions

The method employed in KASCADE-Grande to derive the energy spectrum in the range 10^{16} - 10^{18} eV has been discussed and results presented. The spectrum doesn't show a unique power law. In particular, a break around 10^{17} eV is observed. In order to understand the origin of such feature it is important to understand the evolution of the composition. The different techniques employed by KASCADE-Grande to derive the composition have been briefly discussed. A preliminary result based on the evolution of the *k* parameter, which is sensitive to the evolution of the average mass composition, has been shown using QGSJet II-03 model. Such result indicate that the feature at 10^{17} eV of the all-particle energy spectrum is reflected in the evolution of the *k* parameter.

Acknowledgement: KASCADE-Grande is supported by the BMBF of Germany, the MIUR and INAF of Italy, the Polish Ministry of Science and Higher Education (this work in part by grant for 2009-2011) and the Romanian Authority for Scientific Research.

References

[1] W.-D. Apel et al. (KASCADE Collaboration), Astrop. Phys. **24** (2005) 1.
[2] M. Aglietta et al. (EAS-TOP Coll.), Astrop. Phys. **21** (2004) 583.
[3] V. Berezinsky, A. Gazizov, S. Grigorieva, Phys. Rev D **74** (2006) 043005.
[4] A.M. Hillas, J. Phys. G: Nucl. Part. Phys. **31** (2005) 95.
[5] W.-D. Apel et al. (KASCADE-Grande Collaboration), NIM A **620** (2010) 202.
[6] T. Antoni et al. (KASCADE Coll.), NIM A **513**, 429 (2003).
[7] H. Falcke et al. (LOPES Coll.), Nature **435**, 313 (2005).
[8] F. Schröder et al. (LOPES Coll.), to be published on Astrophys. Space Sci. Trans. (2011).
[9] M. Bertaina et al. (KASCADE-Grande Collaboration), Astrophys. Space Sci. Trans., **8** (2011) 1.
[10] D. Heck et al., Report FZKA 6019, Forschungszentrum Karlsruhe (1998).
[11] A. Fassò et al., Report CERN-2005-10, INFN/TC-05/11, SLAC-R-773 (2005).
[12] S.S. Ostapchenko, Nucl. Phys. B (Proc. Suppl.) **151** (2006) 143&147; S. Ostapchenko, Phys. Rev. D 74 (2006) 014026.
[13] W.-D. Apel et al. (KASCADE Coll.), Astrop. Phys. **24** (2006) 467.
[14] A. A. Lagutin and R. I. Raikin, Nucl. Phys. Proc. Suppl., **97** (2001) 274.
[15] D. Kang, et al. (KASCADE-Grande Collaboration), Proc. 31th ICRC, Lodz - Poland (2009), #icrc1044.
[16] J.-C. Arteaga, et al. (KASCADE-Grande Collaboration), Proc. 31th ICRC, Lodz - Poland (2009), #icrc0805.
[17] V.. de Souza, et al. (KASCADE-Grande Collaboration), Proc. 32th ICRC, Beijing - China (2011), #icrc953.
[18] E. Cantoni, A. Chiavassa et al. (KASCADE-Grande Collaboration), Proc. 32th ICRC, Beijing - China (2011), #0504.
[19] J.-C. Arteaga, A. Chiavassa et al. (KASCADE-Grande Collaboration), Proc. 32th ICRC, Beijing - China (2011), #0739.
[20] D. Fuhrmann et al. (KASCADE-Grande Collaboration), Proc. 32th ICRC, Beijing - China (2011), #0280.